RSC Advances

PAPER

View Article Online
View Journal | View Issue

Cite this: *RSC Adv.*, 2022, **12**, 26023

Hercynite silica sulfuric acid: a novel inorganic sulfurous solid acid catalyst for one-pot cascade organic transformations†

Masoud Mohammadi [a] and Arash Ghorbani-Choghamarani *[b]

Received 5th June 2022
Accepted 1st August 2022

DOI: 10.1039/d2ra03481f

rsc.li/rsc-advances

Herein, we delignated the synthesis of a novel inorganic sulfurous magnetic solid acid catalyst by the immobilization of an extremely high content of sulfuric acid functionalities on the amorphous silica-modified hercynite nanomagnetic core–shell *via* a simple method. Silica sulfuric acid (SSA) modified hercynite nanocomposite (hercynite@SSA) combines excellent recoverability and stability characteristics of hercynite (which can be regarded as a ferro spinel with *Fd*3*m* space group and cubic crystal structure) with the strong Brønsted acid properties of $-SO_3H$ groups. This nanomagnetic solid acid was found to be an efficient and facile strong solid acid catalyst for the synthesis of bis(pyrazolyl)methanes *via* two different one-pot multicomponent methodologies under green conditions. The hercynite@SSA catalyst shows excellent catalytic activity and reusability in the ethanolic medium among different solid acid materials. A plausible reaction mechanism is proposed for this synthesis.

1. Introduction

In recent years, Brønsted acids have played a key role as catalysts or reagents in organic synthesis.[1–3] One of the famous classes of Brønsted acid catalysts is sulfurous acids. Besides, the sulfuric acid catalyst is the most important catalyst for organic reactions *i.e.*, *in situ* generation of the NO_2^+ reagent,[4] the esterification reactions,[5] hydrolysis of esters and carboxylic acids,[6–8] hydration of olefins *etc.*[9] In this context commercially available sulfurous acid catalysts are not convenient due to the problems related to the separation and reusability of the homogeneous catalyst systems.[3,5,10] To overcome these problems, heterogenized solid acid catalysts were developed by Zolfigol *et al.*[11,12] Since 2001, a wide variety of attempts have aimed at bonding various carbonaceous sulfonic acid derivatives to inorganic supports *i.e.* silica, boehmite and alumina were developed using Zolfigol's method, which needs filtration, centrifugation, or other tedious workup procedures to separate these materials from the reaction mixture.[13–16] In some organic reactions, the target products were not dissolved in an optimal solvent; so, they could not be easily separated from the heterogeneous catalyst. Accordingly, organic chemistry methodologists will encounter a complex problem. In this sense, magnetic nanoparticles that can be easily separated from the reaction medium using an external magnetic field, appear as the magic solution to this complex problem.[17–21] Over the last few years, magnetic cores as well as their coating surfaces have been dramatically improved and widely used for different purposes.[22–24]

In recent years, iron aluminate spinel hercynite ($FeAl_2O_4$) has attracted interesting attention as a novel nanomagnetic catalytic support for the heterogenization of homogeneous catalytic species due to many advantages such as high adsorption capacities, large surface area, low cost, heterogeneous nature, paramagnetic nature and excellent physicochemical stability.[25–31] Recently, we have converted this ferro-spinel nanomaterial into a variety of supported active catalytic materials.[32–34] In this context, the present study represents that Zolfigol's SSA catalyst can be efficiently magnetized by being immobilized on the surface of nanomagnetic hercynite. Moreover, the prepared hercynite@SSA nanohybrid system, due to the presence of sulfuric acid on its amorphous surface, can perform organic reactions more easily.

Multi-component reactions (MCRs) can be regarded as a constructive approach to synthesizing heterocyclic compounds with diverse structures.[35–40] In MCRs, the named reactions readily occur in sequence and are often combined.[41] In this sense, the catalytic synthesis including the aldol condensation–Michael addition sequence has been of major interest to researchers in the area of synthetic and methodology chemistry as an important synthetic tool, owing to its ability to synthesize diverse types of heterocyclic compounds using different carbonyl moieties, active hydrogen compounds, and

[a]Department of Chemistry, Faculty of Science, Ilam University, P. O. Box 69315516, Ilam, Iran

[b]Department of Organic Chemistry, Faculty of Chemistry, Bu-Ali Sina University, Hamedan, 6517838683, Iran. E-mail: a.ghorbani@basu.ac.ir; arashghch58@yahoo.com

† Electronic supplementary information (ESI) available: Detailed synthetic procedures, and copies of ^{1}H NMR spectra. See https://doi.org/10.1039/d2ra03481f

Michael donor agents, which will lead to a lot of structural diversity in the final heterocyclic products.[17,41–43]

The functionalized bis(pyrazolyl)methane scaffolds are of great interest due to their various chemical and biological activities.[44] The attractive applications of the functionalized bis(pyrazolyl)methanes have encouraged organic chemists to design numerous synthetic protocols for the synthesis of these pyrazole core-based organic molecules.[45,46] Among them, the one-pot pseudo-five-component and pseudo-three-component reactions have been widely explored and converted to the standard methodologies to evaluate the efficiency of catalytic species.[47,48]

2. Experimental section

2.1. Materials and methods

Chemicals such as $FeCl_2 \cdot 4H_2O$, $Al(NO_3)_2 \cdot 9H_2O$, NaOH, tetraethyl orthosilicate (TEOS), chlorosulfonic acid, phenylhydrazine, ethyl acetoacetate, 3-methyl-1-phenyl-1*H*-pyrazole-5-ol, aldehydes, PEG-400, ethanol, dichloromethane, acetonitrile, methanol, dimethylformamide, acetonitrile and dimethyl sulfoxide were purchased from Merck and Aldrich chemical companies and used as received. The products were characterized by comparison of their spectral data, TLC and physical data.

2.2. Typical procedure for hercynite@SSA preparation

A convenient and inexpensive stepwise procedure was used to prepare hercynite silica sulfuric acid magnetic nanocomposite. In the first step, hercynite MNPs were prepared *via* the typical co-precipitation method, as reported by our group.[49] Afterward, the surface of hercynite was modified using a silica shell according to the Stöber method.[50] Subsequently, 1 g of the obtained hercynite@SiO_2 MNPs was dispersed in 50 mL of dry dichloromethane by sonication for 30 min. Thereafter, the solution was stirred in an ice bath for one hour and, then, 1.5 mL of chlorosulfuric acid reagent was added dropwise and stirred for 4 h at room temperature to ensure the complete consumption of the surface hydroxyl groups and assist the sulfuric acid immobilization. After completion of the reaction (when the release of HCL gas from the reaction vessel was stopped), the reaction mixture was separated using magnetic decantation and, then, washed thrice with dry dichloromethane. The obtained hercynite@SSA MNPs were then dried at room temperature (Scheme 1).

2.3. General procedures for the synthesis of bis(pyrazolyl) methanes

In a general reaction, 15 mg of hercynite@SSA catalyst was added to a 5 mL ethanol solution of aryl aldehydes (1 mmol) and (i) commercial 3-methyl-1-phenyl-1*H*-pyrazole-5-ol (2 mmol) (pseudo-three-component, Scheme 2a) or (ii) synthetic mixture of phenylhydrazine (2 mmol) ethyl acetoacetate (2 mmol) (pseudo-five-component, Scheme 2b) in 10 mL round bottom flask and, then, the resulting solution was stirred for the appropriate time at reflux conditions (80 °C). After completion of the reaction (probed by TLC), the hercynite@SSA MNPs were separated from the boiling mixture using magnetic decantation. The precipitated bis(pyrazolyl)methanes were purified by recrystallization in ethanol thrice. The isolated pure products, known in the literature, were authenticated by their corresponding melting points and also the performed ^{1}H-NMR spectroscopies as reported in ESI.†

3. Results and discussions

3.1. Synthesis and characterization of hercynite@SSA

Hercynite@SSA nanocomposite was prepared *via* a multistep process as described in Scheme 1. To prove the formation of amorphous silica shell and immobilization of SO_3H groups on

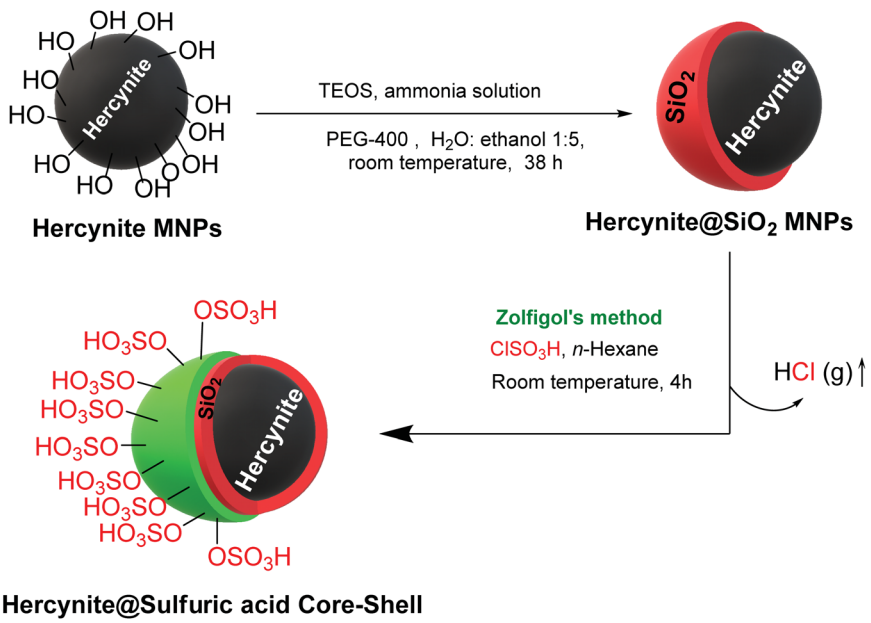

Scheme 1 Stepwise synthesis of hercynite@SSA.

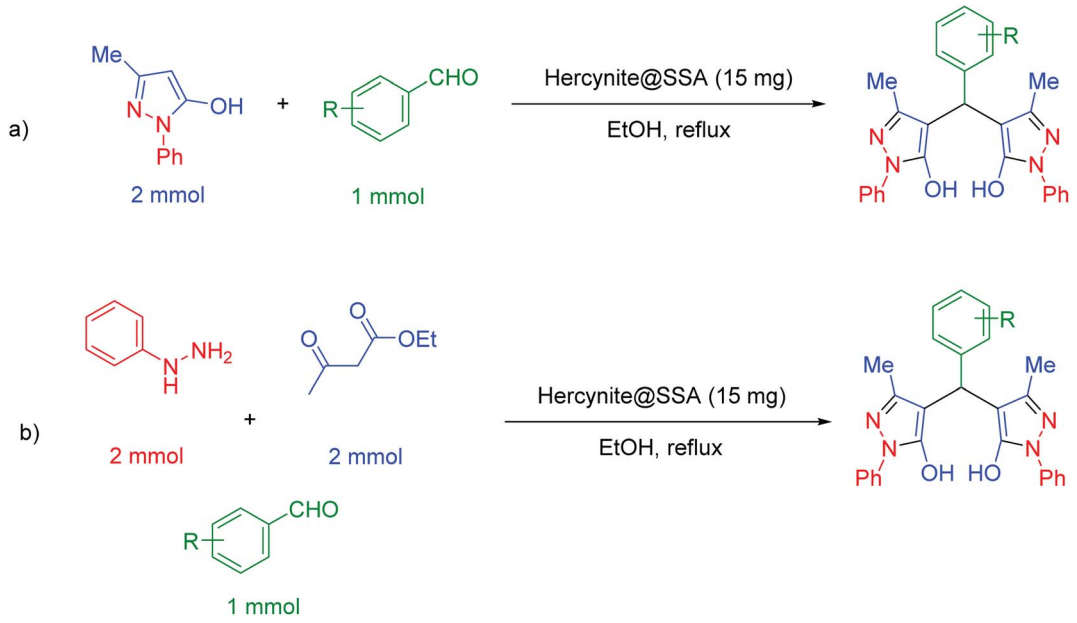

Scheme 2 The (a) pseudo-three-component and (b) pseudo-five-component synthesis of bis(pyrazolyl)methanes catalyzed by hercynite@SSA.

the magnetic hercynite NPs, the FT-IR, XRD, TGA, DSC, EDX, X-ray mapping, SEM, TEM, VSM and BET analyses were provided.

The FT-IR spectra of (a) hercynite, (b) hercynite@SiO_2 and (c) hercynite@SSA nanocomposites are shown in Fig. 1. Regarding the FT-IR spectrum of the hercynite, the bands at 722 cm^{-1}, 580 cm^{-1} and 450 cm^{-1} are attributed to the Al–O and Fe–O vibrations, respectively, which are clear indications for the formation of the hercynite MNPs.[25] In addition, the broadband observed at 3430 cm^{-1} corresponds to the stretching vibrations of –OH groups.[25] In the case of hercynite@SiO_2 core–shell, the appearance of broad bands at around 1089 cm^{-1} and 800 cm^{-1} are attributed to the Si–O and Si–O–Si stretching vibrations, respectively,[51,52] confirming the successful formation of the amorphous silica shell over the nanomagnetic hercynite core. In the fingerprint spectrum of the hercynite@SSA, the broadband at 3436 cm^{-1} appeared due to O–H group in sulfonic acid.[53] Moreover, the important bands at 1632 cm^{-1}, 1237–994 cm^{-1} and 580 cm^{-1} also appeared due to the S=O and S–O vibrations respectively,[54] which show that the symmetric and symmetric expanding bands of SO_2 imbricated with Si–O–Si expanding bands in the silica shell. These significant bands indicate the successful immobilization of SO_3H groups over hercynite@SiO_2 nanomagnetic core–shell support.

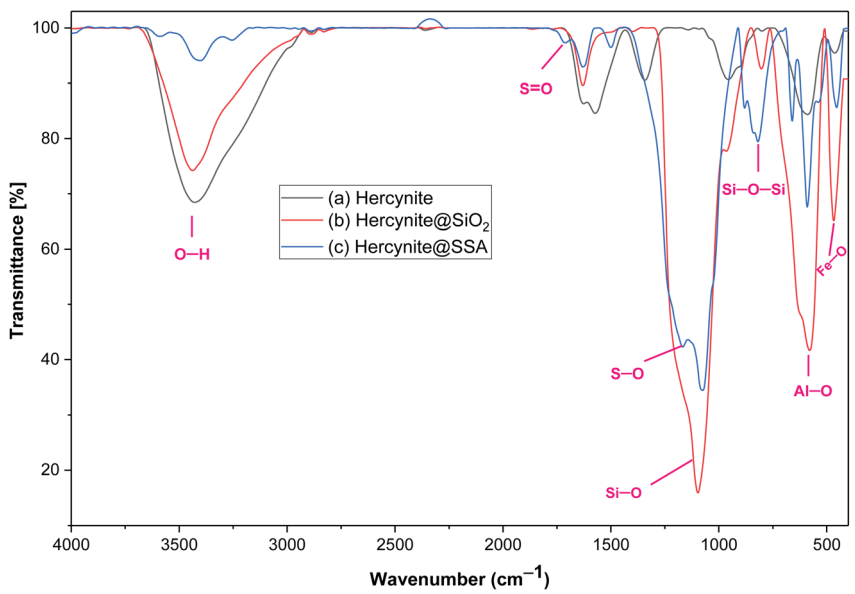

Fig. 1 The FT-IR spectra of (a) hercynite, (b) hercynite@SiO_2 and (c) hercynite@SSA MNPs.

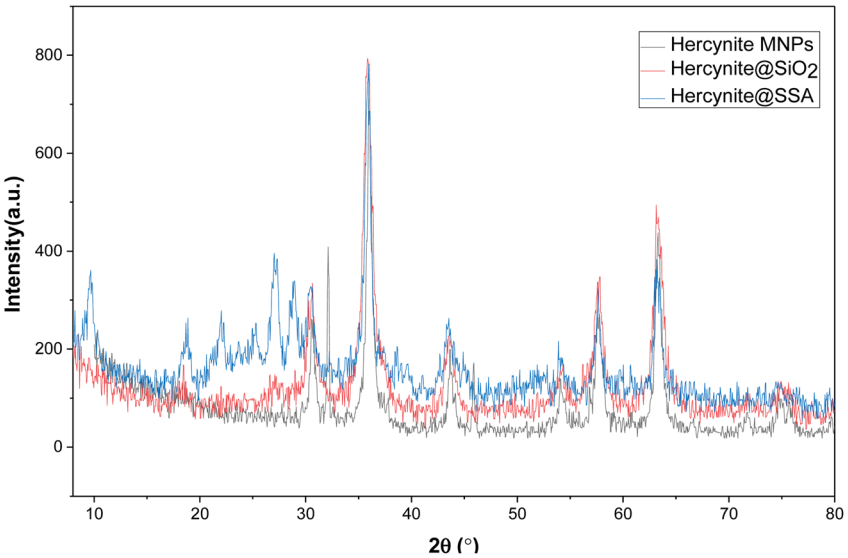

Fig. 2 The XRD patterns of hercynite, hercynite@SiO_2, and hercynite@SSA MNPs.

The X-ray diffraction patterns of the as-synthesized (a) hercynite, (b) hercynite@SiO_2, (c) hercynite@SSA nanocomposites are shown in Fig. 2. In this context, the existence of individual sharp peaks in the depicted XRD patterns represents that all the examined composite systems have the extent of crystallinity character. In this context, the P-XRD pattern of hercynite MNPs accords with the XRD pattern of the crystalline cubic spinel normal mineral hercynite ($FeAl_2O_4$) and agrees with the standard of (JCPDS file, PDF no. 96-901-2447).[55] Moreover, the XRD pattern of hercynite@SiO_2 represents that besides the all-diffraction peaks of nano hercynite, the position of a broad peak which appeared at $2\theta = 18–29°$ is due to the short-range order structure.[56] Besides, it also discloses the presence of an amorphous phase of silica nano-phase segments, which generally occurs due to the surface stabilized SiO_2 shell indicating that the surface of magnetic core–shell particles is amorphous in structure. The P-XRD pattern of hercynite@SSA represents that, after adding the SO_3H functionalities, some new peaks appeared at $2\theta = 22–30°$ confirming the successful surface functionalization by acidic species.[57] In addition, the peaks corresponding to the structure of hercynite@SiO_2 exist in the XRD pattern of hercynite@SSA, which shows that the nanomagnetic core–shell structure is not destroyed after the immobilization of acidic sites.

Thermogravimetric analysis (TGA) and differential scanning calorimetry (DSC) of hercynite, hercynite@SiO_2 and

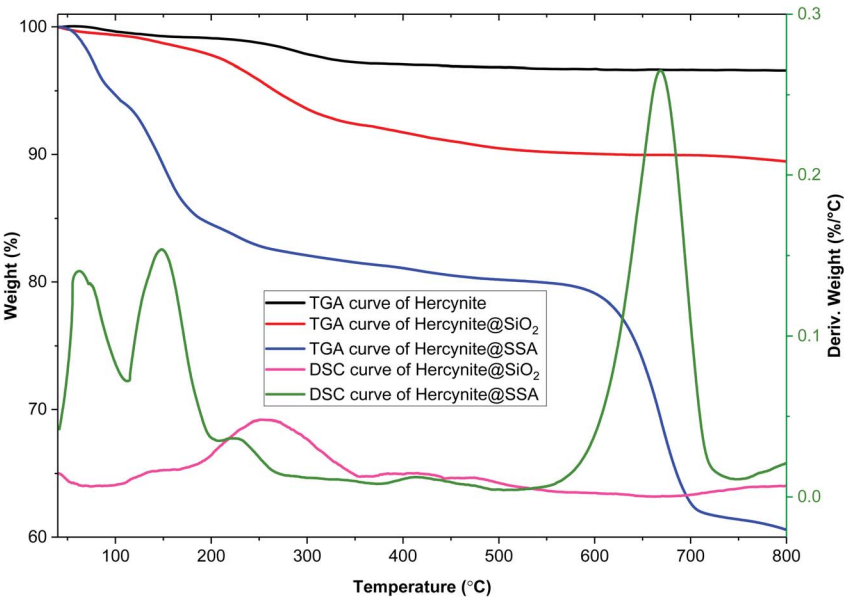

Fig. 3 TGA and DSC analysis of hercynite, hercynite@SiO_2 and hercynite@SSA MNPs.

hercynite@SSA nanohybrid materials were applied to investigate the weight loss and stability of the immobilized amorphous phase of silica and silica sulfuric acid segments on hercynite (Fig. 3). In the case of hercynite@SiO_2, the depicted TGA and DSC curves show the initial 2.25% mass loss in the area of 50–200 °C that is attributed to the presence of organic solvents and moisture adsorbed on the surface of the nanocomposite. Moreover, the next weight loss at about 8% above 200 °C indicates removing of organic moieties such as PEG-400 and the surface hydroxyl groups by the vaporization and oxidative decomposition of volatile products from the immobilized amorphous phase of silica segment.[58–60] In addition, at above 350 °C, no weight loss was observed confirming the thermal stability of the prepared nanocomposite. DSC analysis indicated that the hercynite@SiO_2 nanocomposite has good thermal stability. The TGA and DSC curves of hercynite@SSA MNPs show that the 18 wt% of the sample contains volatile solvents and surface hydroxyl groups that were removed in three consecutive steps at below 300 °C.[58] The single-step endothermic mass loss corresponding to 18.17% at the region of 550–720 °C occurs due to the degradation of the chemisorbed sulfuric acid functionalities in the SSA layer on the surface of hercynite core.[61,62] These findings represent the successful synthesis of the targeted hercynite@SSA catalyst and its thermal stability under aerobic conditions up to 550 °C, making it a magnetically superior and recoverable solid acid catalyst for industrial applications.

The elemental composition of the synthesized hercynite@SiO_2 and hercynite@SSA nanocomposites was carried out using EDX analysis. The EDX measurements indicate that all of the required elements, including Fe (Lα = 0.705, kα = 6.398 and kβ = 7.07 keV), Al (kα = 1.486 keV), O (kα = 0.525 keV) and Si (kα = 1.739 keV) species in hercynite@SiO_2 MNPs, confirm the formation of the amorphous phase of silica shell over the nanomagnetic hercynite core. Additionally, the EDX measurements on hercynite@SSA represent that, besides all of the X-ray signals of hercynite@SiO_2, the position of a sharp peak of sulfur (Kα = 2.32 keV) element is attributed to SO_3H segments. The EDX curve of hercynite@SSA also shows that the intensities and quantities of Fe Lα and Si kα signals decreased in comparison to its hercynite@SiO_2 parent, which is due to the addition of SO_3H functionalities that lead to change in the chemical composition and weight percentage of nanocomposite elements. These results and the absence of chlorine signal suggest the chemisorption of inorganic sulfurous acid functionalities on the surface of the hercynite@SiO_2 nanoparticles and the successful formation of the target catalytic complex. Moreover, the exact amount of sulfur in the catalyst is 7.72 wt% (Fig. 4).

The typical amount of SO_3H groups in the hercynite@SSA was determined by acid–base titration of its conjugate acid (H_3O^+) in aqueous solution using standard NaOH, which is a standard method for acidity determination in solid catalysts.[63,64] As measured *via* titration of the SO_3H groups, the amount of H^+ in hercynite@SSA was found to be 0.95 mmol per 0.05 g of hercynite@SSA.

In addition, the distribution of the elements was investigated using EDX-mapping analysis (Fig. 5). Elemental mapping images revealed a high density of Fe, Al, and O elements as the magnetic core and high content of Si elements were uniformly distributed around the composite system, confirming the formation of the hercynite@SiO_2 core–shell. In addition, the uniform distribution of sulfur species in hercynite@SSA shows that the sulfuric acid functionalities have evenly linked to the surface of hercynite@SiO_2 core–shell support. It was observed that the reported synthesis approach assists in giving good

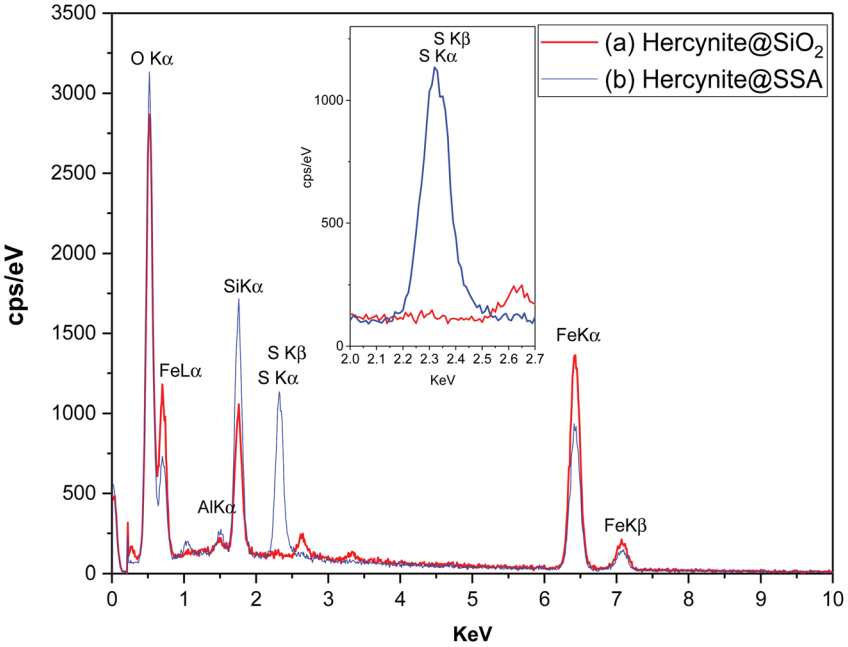

Fig. 4 EDX analysis of hercynite@SiO_2 and hercynite@SSA MNPs.

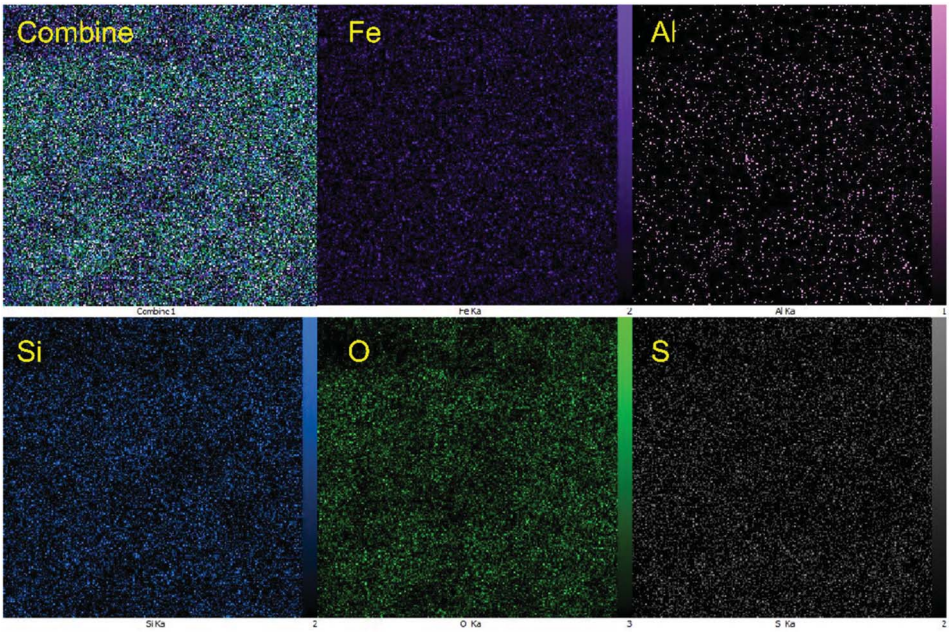

Fig. 5 X-ray mapping images of hercynite@SSA MNPs.

control over the morphology, nano size and dispersibility, and accessibility of the catalytic sites under the surface of MNPs.

The morphology and size of (a) hercynite, (b) hercynite@SiO_2, and (c) hercynite@SSA were evaluated using FE-SEM analysis as shown in Fig. 6. The comparison of SEM images confirmed that the immobilization of silica shells and sulfurous acid moieties on hercynite MNPs was successful. In this regard, it is worth mentioning that hercynite MNPs have a monodispersed spherical morphology with an average particle size of 26 nm, which causes the good distribution of the amorphous phase of silica shell and sulfuric acid species on the support surfaces. In the case of hercynite@SiO_2 core–shell, the FE-SEM micrographs show the monodispersed spherical shape particles with an increase in the average particle size (37 nm) due to the formation of SiO_2 shell over the hercynite core. In addition, the hercynite@SSA morphology shows some accumulation and agglomeration of the particles due to strong chemical adsorption and functionalization of the sulfuric acid moieties onto the amorphous silica shell, which provides better stabilization to the formed particles. The size of hercynite@SSA MNPs was found to be larger as compared to silica-modified hercynite nanocomposite. These observations confirm the successful formation of SSA over the hercynite MNPs.

The shape, size and morphology of the designed hercynite@SSA MNPs were determined using transmission electron microscopy (TEM). The TEM images of spherical-shaped ferrite materials with smooth surface is shown in Fig. 7 in different magnification. The form of these materials is that of a homogeneous amorphous phase of silica shell that is uniformly dispersed over the surface of spinel normal hercynite core. No noticeable morphological change is observed instead of surface roughening of a slight agglomeration of ferrite nanoparticles that caused by the addition of sulfuric acid functional groups. TEM images provides an additional information about the average size of magnetite nanoparticles which is found to be 47 nm. Besides, TEM images reveals SiO_2 crust size over the hercynite as ultrathin layers of thickness 7.5–14 nm on an average, which is due to the formation of amorphous catalytic phase around the particles. Further, increase in size of bare hercynite and formation of light shell over the core, strongly justify the fact that SO_3H functionalities along with the SiO_2 moieties has been immobilized on to its surface.

The magnetic property and value of (a) hercynite, (b) hercynite@SiO_2 and (c) hercynite@SSA nanocomposites were further evaluated using VSM measurements at room temperature (Fig. 8). The saturation magnetization (M_s) values of (a) hercynite, (b) hercynite@SiO_2, and (c) hercynite@SSA are respectively 40, 28, and 25 emu g^{-1}. The values clearly show that, through surface modification and catalytic functional group immobilization on hercynite support, the magnetization value of samples was intensively diminished. Nevertheless, the targeted MNPs presented excellent superparamagnetism and can be separated easily.

BET isotherm analysis provides another testimony for the incorporation of silica sulfuric acid on hercynite (Fig. 9). The results show that with a pore diameter 40.513 nm, total pore volume 0.055327 [cm^3 g^{-1}] and the quantity adsorbed in this BET surface area 1.2551 [cm^3 (STP) g^{-1}], this novel heterogeneous acid catalyst exhibits a highest BET specific surface area of 5.4626 [m^2 g^{-1}] at a temperature of 77 K. As shown in Fig. 9, hercynite@SSA is classified as a type IV isotherm.

3.2. Catalytic properties of hercynite/SSA

3.2.1. Reaction of 4-chlorobenzaldehyde with phenylhydrazine and ethyl acetoacetate. We investigated the catalytic

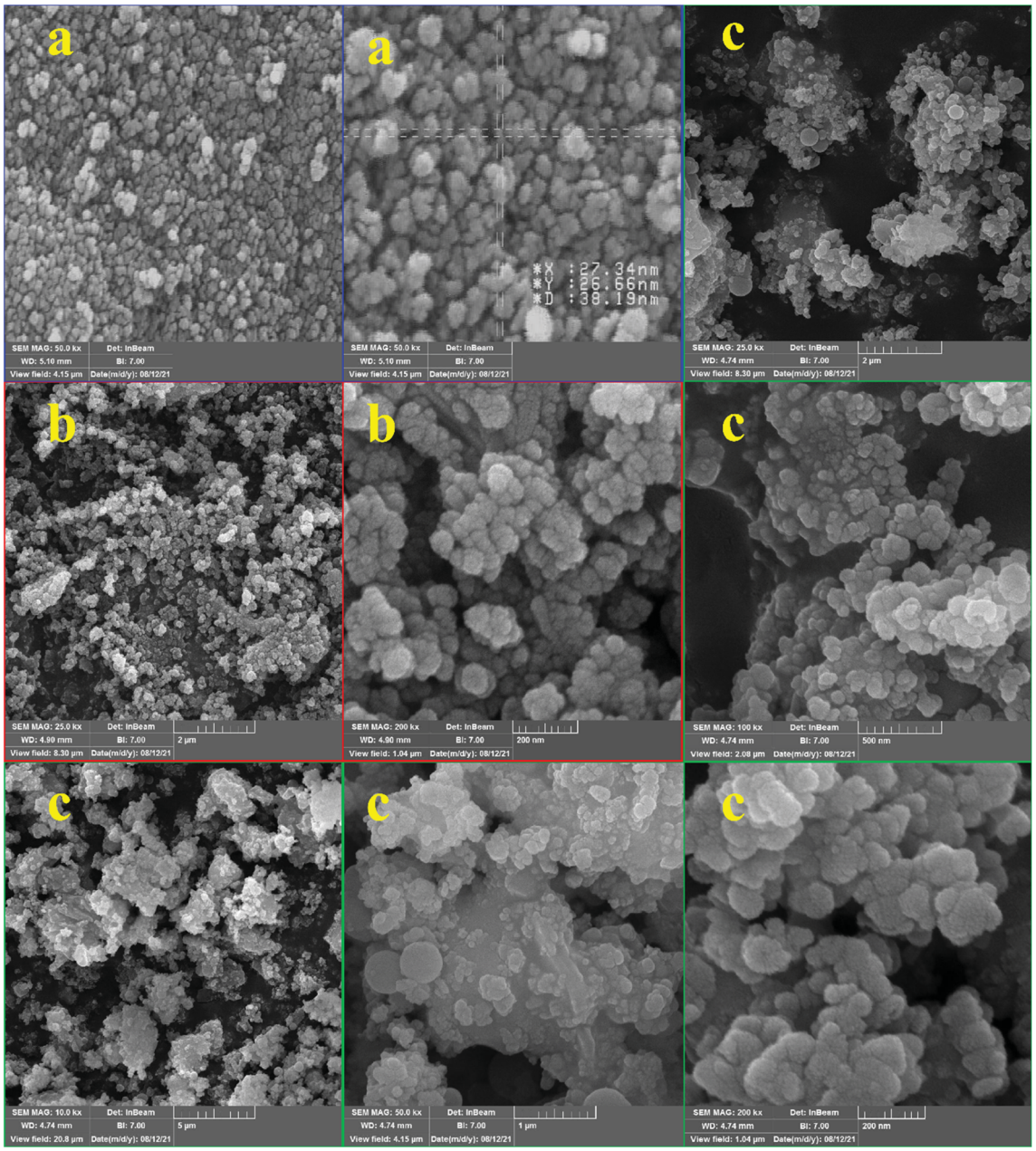

Fig. 6 SEM images of (a) hercynite, (b) hercynite@SiO_2 and (c) hercynite@SSA MNPs.

performance of hercynite@SSA by selecting the pseudo-five-component reaction of 4-chloro benzaldehyde to generate its corresponding bis(pyrazolyl)methane as a probe reaction. The effect of catalysis parameters on the transformation process was optimized using the controlled variable method. In the first step, the effect of catalyst-free condition on the reaction was examined, and, after 10 h, the TLC results indicated no product formation as shown in Table 1 entry 1. The catalytic activity of hercynite and hercynite@SiO_2 was also examined and trace amounts of products were obtained in long reaction times and both of these nanomagnetic materials show low catalytic activity in this reaction (Table 1 entries 2 and 3). We conducted the same reaction with sulfunated hercynite@SiO_2 (hercynite@SSA) as the catalyst to explore the potential of our designed inorganic sulfurous solid acid material, after the addition of SO_3H functionalities to the catalyst, an increase in reaction yield occurred (Table 1 entry 4). Hercynite@SSA has the best catalytic activity among these nanomaterials. Afterward, the amount of hercynite@SSA was varied to determine its effect on the reaction progress as shown in Table 1 entries 4–9. When 15 mg of the catalyst was taken, the complete transformation of reactants took place in 120 min (Table 1 entry 7). It was observed that on increasing the amount of catalyst the reaction yields also increased. For instance, when the catalyst amount was 5 mg the reaction yield was 34% and we also witnessed 63, 89 and 97% for 8, 10 and 15 mg, respectively (Table 1 entries 4–7).

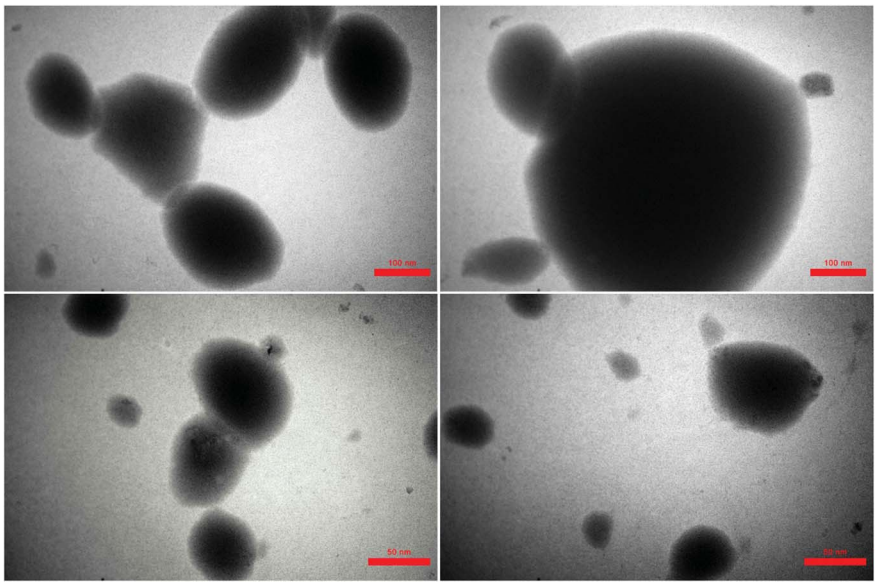

Fig. 7 TEM images of hercynite@SSA MNPs at different magnification.

However, on further increasing the amount to 20 mg, there was no drastic change in reaction yield (Table 1, entry 8). Hence, 15 mg was selected as the optimum catalyst amount for further experiments. Subsequently, the effect of solvent was examined, and, accordingly, the investigation of the results exhibited that among the examined solvents including EtOH, CH_3CN, MeOH, H_2O, DMSO, DMF, and solvent-free conditions the model reaction shows perfect efficiency in refluxing EtOH using 15 mg of the solid acid catalyst (Table 1, entry 7). In the case of water, the low solubility of reactants in water as a solvent proceeds the reaction with a lower rate and efficiency. It is worth to mention that, the reaction efficiency was decreased as the amount of water present in the medium increased going from ethanol to methanol and water. The deactivating effect of water also manifested itself by changes in the activation energy. Moreover, the decreased activity of the catalytic protons is suggested to be caused by preferential solvation of them by water.[33] Moreover, the reaction did not proceed to any extent without solvent (Table 1, entry 13). Finally, the effect of temperature on the performance of the reaction was also evaluated. The negative results were obtained with hercynite@SSA catalyst at room temperature in presence of ethanol as the optimal solvent (Table 1, entry 15). Additionally, the reaction proceeded smoothly at 60 °C (Table 1, entry 16). Based on the observations,

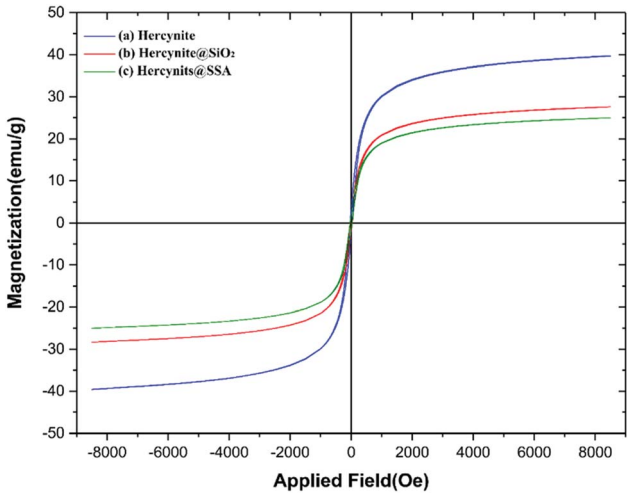

Fig. 8 VSM analysis of (a) hercynite, (b) hercynite@SiO_2 and (c) hercynite@SSA MNPs.

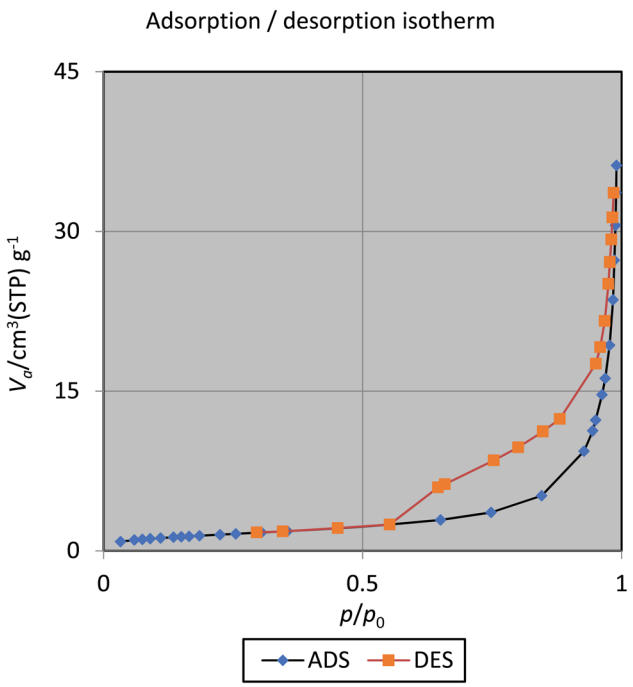

Fig. 9 BET plot of the nitrogen adsorption–desorption isotherms of hercynite@SSA MNPs.

Table 1 Screening the reaction parameters for the pseudo-five-component synthesis of bis(pyrazolyl)methanes under the catalysis of hercynite@SSA

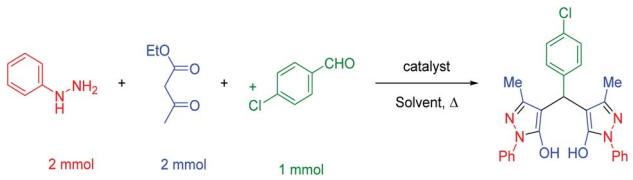

Entry	Catalyst	Catalyst amount (mg)	Solvent	Temperature (°C)	Time (min)	Yield[a,b] (%)
1	—	—	EtOH	Reflux	600	NR
2	Hercynite	15	EtOH	Reflux	600	Trace
3	Hercynite@SiO_2	15	EtOH	Reflux	600	Trace
4	Hercynite@SSA	5	EtOH	Reflux	120	34
5	Hercynite@SSA	8	EtOH	Reflux	120	63
6	Hercynite@SSA	10	EtOH	Reflux	120	89
7	Hercynite@SSA	15	EtOH	Reflux	120	97
8	Hercynite@SSA	20	EtOH	Reflux	120	97
9	Hercynite@SSA	15	CH_3CN	Reflux	120	93
10	Hercynite@SSA	15	MeOH	Reflux	120	91
11	Hercynite@SSA	15	Water	Reflux	120	46
12	Hercynite@SSA	15	DMF	100	120	88
13	Hercynite@SSA	15	Solvent-free	100	120	71
14	Hercynite@SSA	15	DMSO	100	120	90
15	Hercynite@SSA	15	EtOH	25	120	Trace
16	Hercynite@SSA	15	EtOH	60	120	81

[a] Isolated yield. [b] Conditions: phenylhydrazine (2 mmol), ethyl acetoacetate (2 mmol) and 4-chlorobenzaldehyde (1 mmol), catalyst (mg), and solvent (5 mL).

15 mg of the catalyst in refluxing ethanol was considered the optimum condition for the reaction.

3.2.2. Synthesis of the bis(pyrazolyl)methane derivatives. This outcome enhanced our attention to study the scope, generality, and relevance of this protocol for the synthesis of bis(pyrazolyl)methanes derivatives. In this sense, two comparative studies including (a) one-pot pseudo-five-component (phenylhydrazine, ethyl acetoacetate, and aryl aldehydes (2 : 2 : 1)) and pseudo-three-component (3-methyl-1-phenyl-1*H*-pyrazole-5-ol and aryl aldehydes (2 : 1)) synthetic procedures were evaluated and, then, a series of aryl-functionalized bis(-pyrazolyl)methanes was synthesized using a variety of structurally relevant aldehydes under the optimized conditions as mentioned in Table 2. The table represents that both of these synthetic protocols worked very well with aldehydes containing electron-deficient and electron-rich substituents using 15 mg of hercynite@SSA in refluxing EtOH. All reactions were carried out in 25–195 min to afford the corresponding products in high yields (87–99%). In the case of aldehyde compounds containing electron-withdrawing functionality, the reactions were faster than in the case of aryl aldehydes having electron-donating groups. In this sense, it can be due to the activation or deactivation effect of functionalities of the aryl ring on the reactivity of aldehyde and the generated α,β-unsaturated intermediate. However, various factors such as electronic and steric hindering of reactants and intermediates are the limitations responsible for the observed difference in the reactivity of the studied reactions. Finally, the results of these investigations indicated that the catalytic pseudo-three-component reaction was faster and took lesser time than the pseudo-five-component synthetic method, and provided the corresponding products in higher yields. The exact explanation for this difference in efficiency is due to the formation of ethanol-soluble by-products through the *in situ* formation of 3-methyl-1-phenyl-1*H*-pyrazole-5-ol *via* the acidic aminolysis of ethyl acetoacetate using phenylhydrazine, which prevents the progress and completion of the further cascade reaction towards the formation of the bis(pyrazolyl)methane products.

3.2.3. Proposed reaction mechanism. The plausible mechanism of hercynite@SSA of synthesis of bis(pyrazolyl) methanes, as illustrated in Scheme 3.[47] According to the previous reports, it was found that sulfurous acids have been proven as an efficient catalyst to mediate organic reactions in ethanolic medium.[33] Hercynite@SSA was found to act as a proton donor through a hydrogen bonding mechanism. At first, hydrogen bonding activated the ethyl acetoacetate carbonyls in presence of hercynite@SSA nanocatalyst and, then, 1-phenyl-1*H*-pyrazole-5-ol was produced from the aminolysis reaction. As reported in the literature, the catalytic reaction of an enol or an enolate ion with the aldehydes generates a β-

Table 2 Synthesis of the bis(pyrazolyl)methane derivatives catalyzed by hercynite@SSA

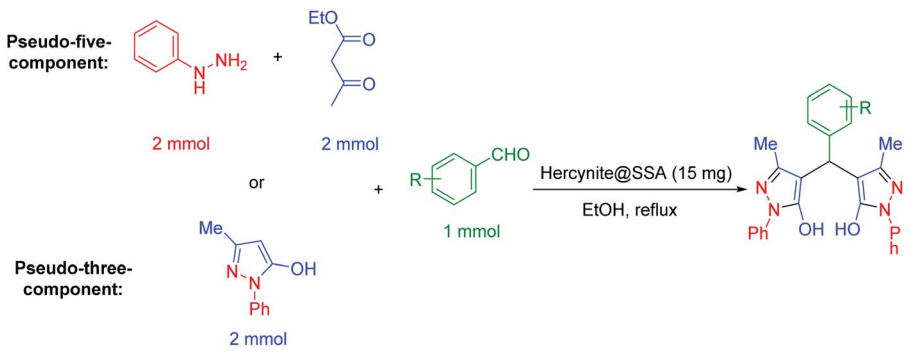

Entry	Synthesis type	Aldehyde	Product	Time (min)	Yield[a,b] (%)	Melting point (°C) Measured	Melting point (°C) Literature
1	Pseudo-five-component	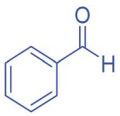	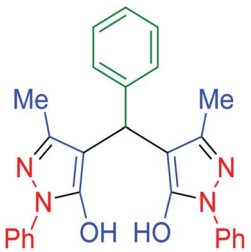	85	95	170–172	170–172 (ref. 65)
2	Pseudo-three-component	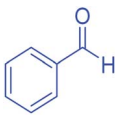	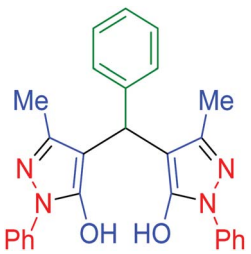	35	97	170–172	170–172 (ref. 65)
3	Pseudo-five-component	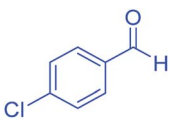	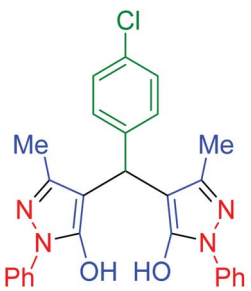	120	97	213–215	213–215 (ref. 66)
4	Pseudo-three-component	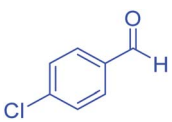	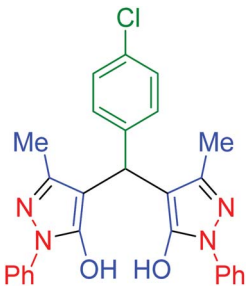	45	99	213–215	213–215 (ref. 66)

Table 2 (*Contd.*)

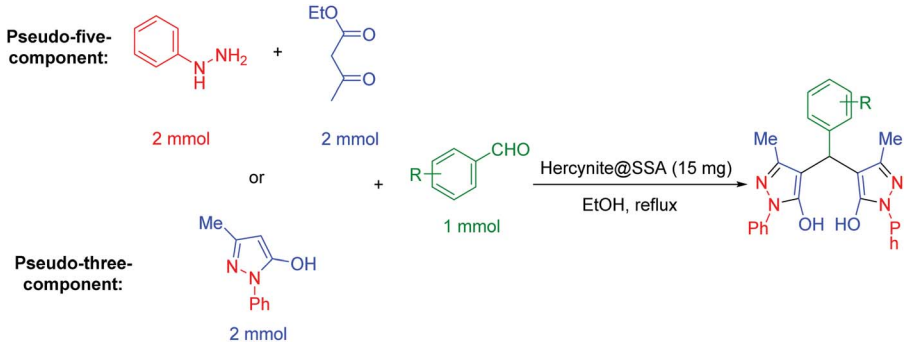

Entry	Synthesis type	Aldehyde	Product	Time (min)	Yield[a,b] (%)	Melting point (°C) Measured	Melting point (°C) Literature
5	Pseudo-five-component	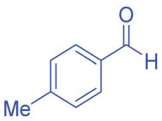	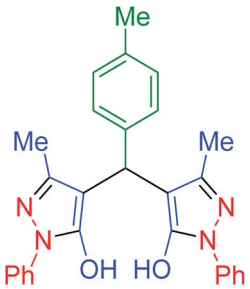	120	95	202–204	202–204 (ref. 65)
6	Pseudo-three-component	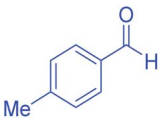	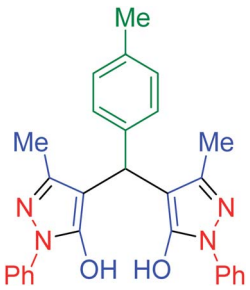	55	97	202–205	202–204 (ref. 65)
7	Pseudo-five-component	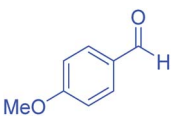	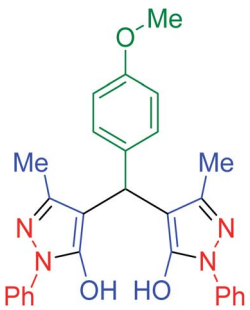	135	92	173–175	173–175 (ref. 66)
8	Pseudo-three-component	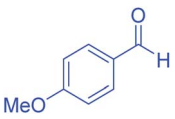	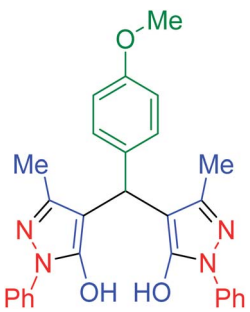	60	95	171–173	173–175 (ref. 66)

Table 2 (*Contd.*)

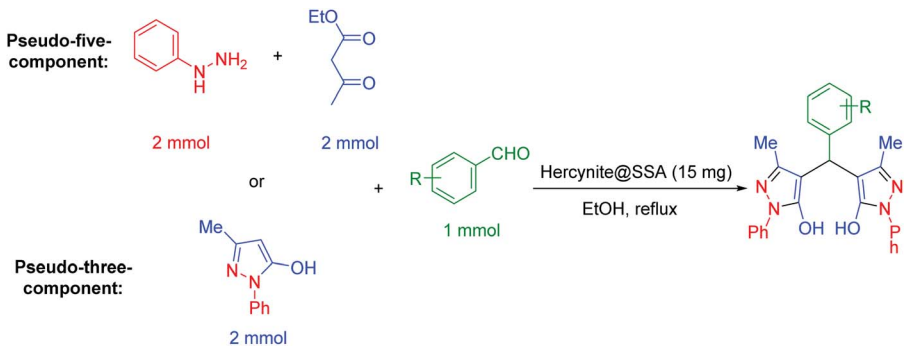

Entry	Synthesis type	Aldehyde	Product	Time (min)	Yield[a,b] (%)	Melting point (°C) Measured	Melting point (°C) Literature
9	Pseudo-five-component	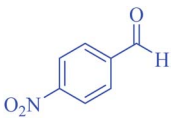	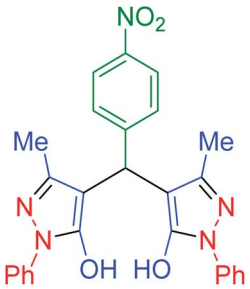	90	93	226–228	225–227 (ref. 67)
10	Pseudo-three-component	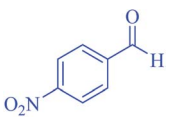	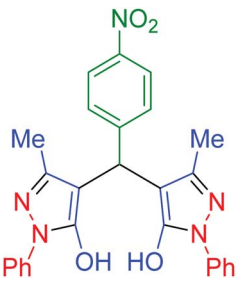	25	97	225–226	225–227 (ref. 67)
11	Pseudo-five-component	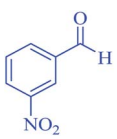	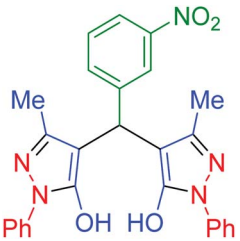	150	92	151–153	151–153 (ref. 68)
12	Pseudo-three-component	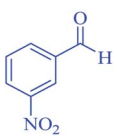	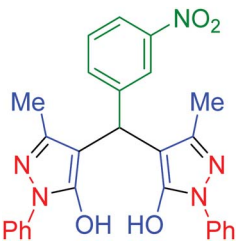	45	96	151–153	151–153 (ref. 68)

Table 2 (*Contd.*)

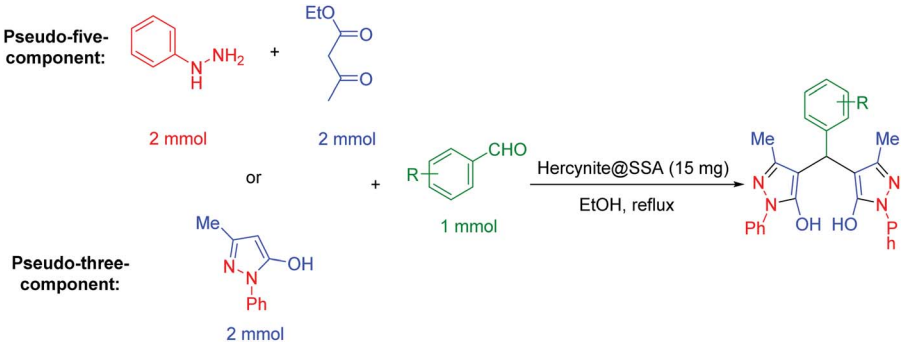

Entry	Synthesis type	Aldehyde	Product	Time (min)	Yield[a,b] (%)	Melting point (°C) Measured	Melting point (°C) Literature
13	Pseudo-five-component	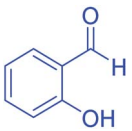	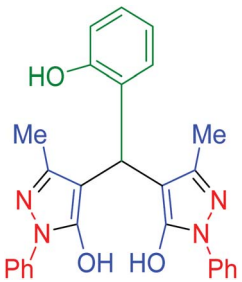	160	89	215–217	216–217 (ref. 69)
14	Pseudo-three-component	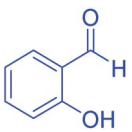	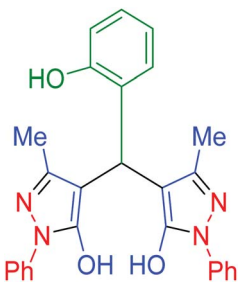	85	92	216–218	216–217 (ref. 69)
15	Pseudo-five-component	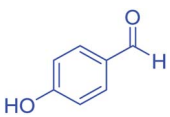	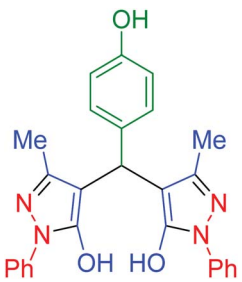	140	91	154–156	153–155 (ref. 66)
16	Pseudo-three-component	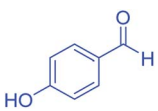	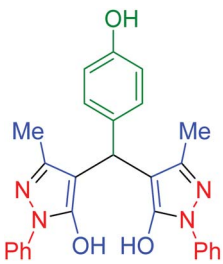	60	93	153–155	153–155 (ref. 66)

Table 2 (*Contd.*)

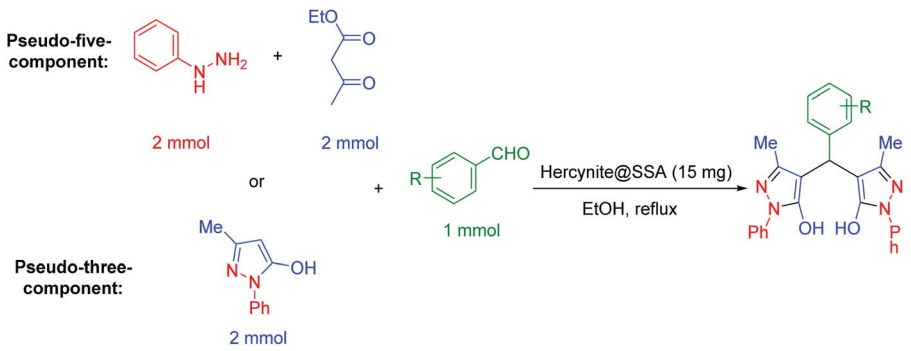

Entry	Synthesis type	Aldehyde	Product	Time (min)	Yield[a,b] (%)	Melting point (°C) Measured	Melting point (°C) Literature
17	Pseudo-five-component	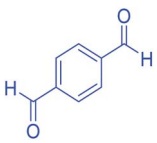	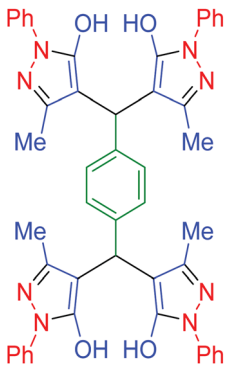	110	93	210–213	211–215 (ref. 70)
18	Pseudo-three-component	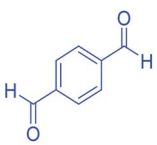	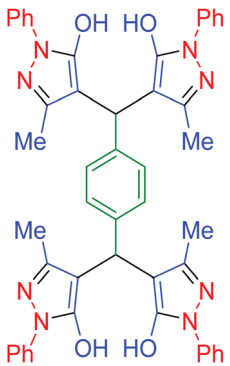	85	95	211–214	211–215 (ref. 70)
19	Pseudo-five-component	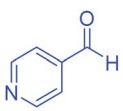	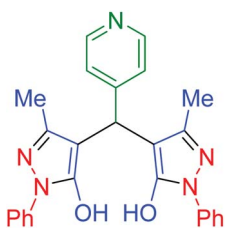	180	94	248–250	248–250 (ref. 71)
20	Pseudo-three-component	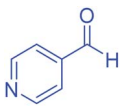	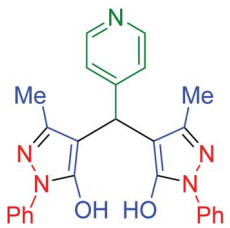	100	97	247–250	248–250 (ref. 71)

Table 2 (*Contd.*)

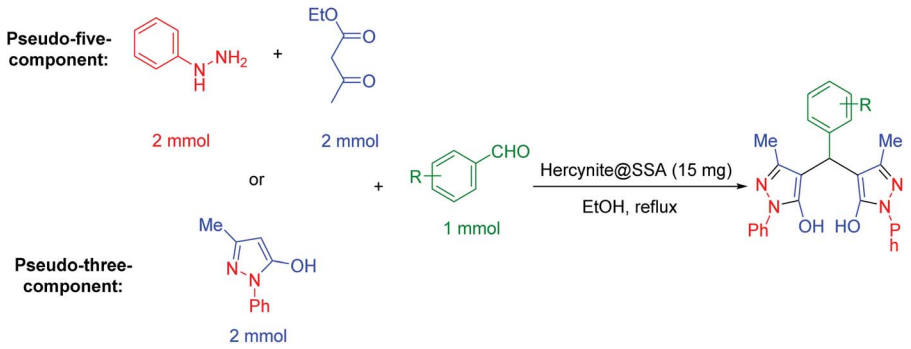

Entry	Synthesis type	Aldehyde	Product	Time (min)	Yield[a,b] (%)	Melting point (°C) Measured	Melting point (°C) Literature
21	Pseudo-five-component	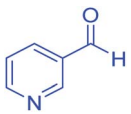	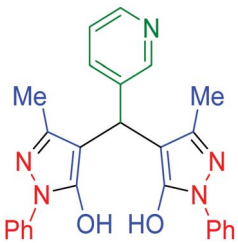	195	87	238–239	238–239 (ref. 72)
22	Pseudo-three-component	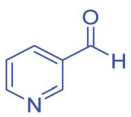	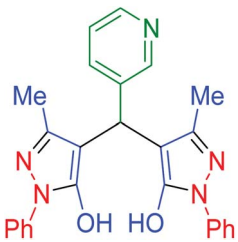	120	89	238–240	238–239 (ref. 72)
23	Pseudo-five-component	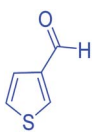	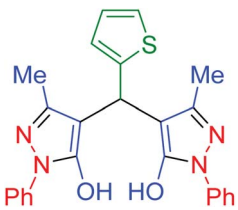	165	90	187–190	187–190 (ref. 69)
24	Pseudo-three-component	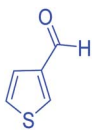	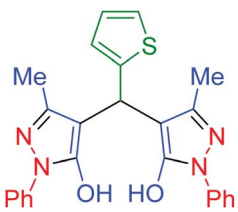	110	92	188–190	187–190 (ref. 69)

[a] Isolated yield. [b] Conditions: (a) one-pot pseudo five-component: phenylhydrazine (2 mmol), ethyl acetoacetate (2 mmol) aryl aldehydes (1 mmol) and hercynite@SSA (15 mg) in EtOH (5 mL) under reflux conditions. (b) One-pot pseudo three-component: aryl aldehyde (1 mmol), 1-phenyl-1*H*-pyrazole-5-ol (2 mmol) and hercynite@SSA (15 mg) in EtOH (5 mL) under reflux conditions.

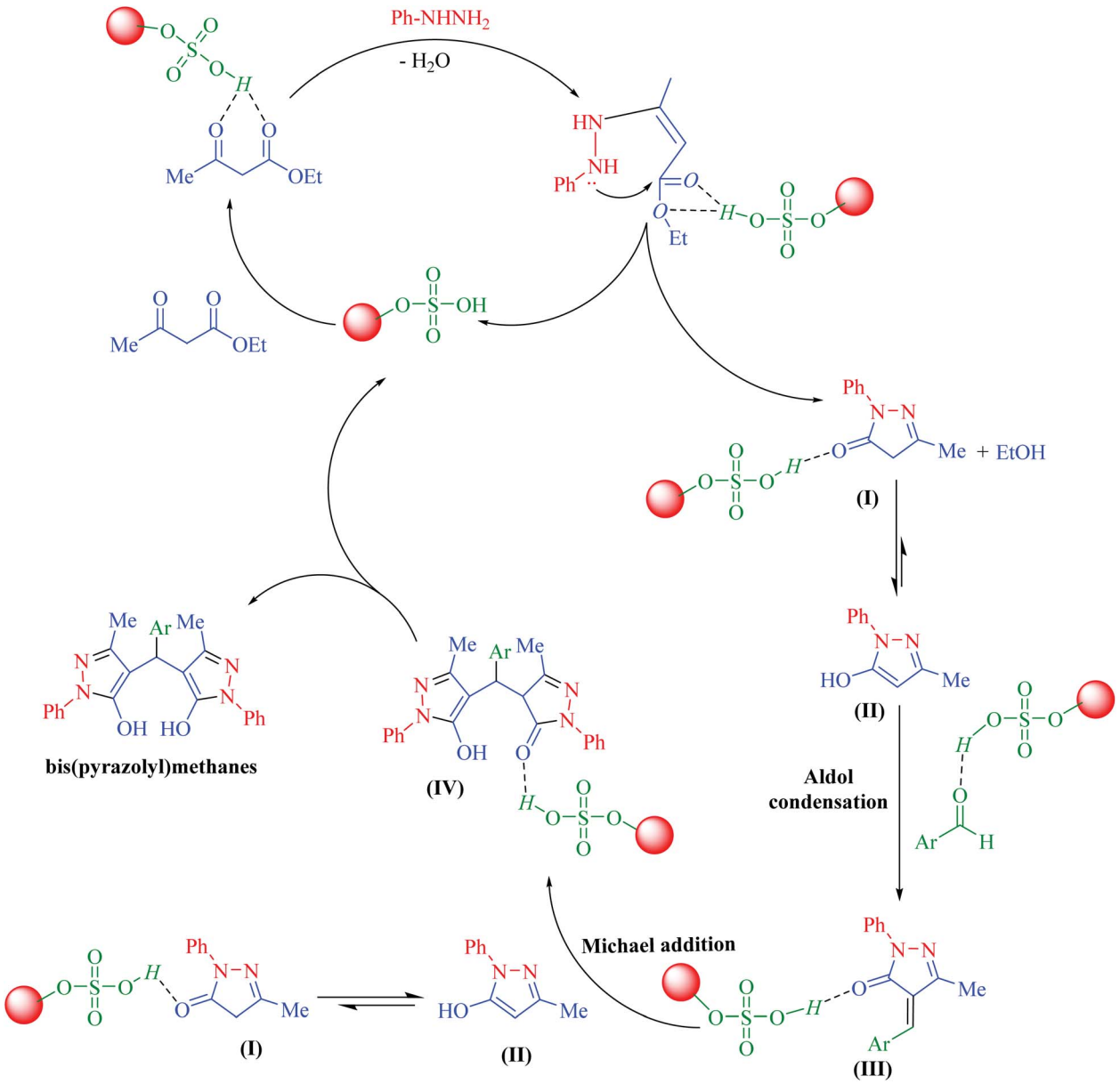

Scheme 3 Plausible mechanism for the synthesis bis(pyrazolyl)methanes catalyzed by hercynite@SSA.

hydroxy ketone followed by the removal of a water molecule to give a β-unsaturated compound (III) *via* aldol condensation.[43] In this process, the hercynite@SSA acts as the catalytic system, where the electrons can be transferred from the enol moiety to the aldehyde group. The α,β-unsaturated structural setup of conjugated enone leads to an increase in the electron transfer between aryl, alkene, and keto groups. This, in turn, may also lead to the susceptibility of the formation and reactivity of this intermediate from the functional groups in the aryl ring. Subsequently, the catalytic conjugate addition of another equivalent of enone to aldol intermediate (III), followed by tautomerization (1,3-H shift) of intermediate IV, provides the corresponding bis(pyrazolyl)methane products.[47]

3.2.4. Stability of hercynite/SSA

3.2.4.1. Cyclic test. Regarding features of sustainability and green chemistry, recovery and reusability of the heterogeneous

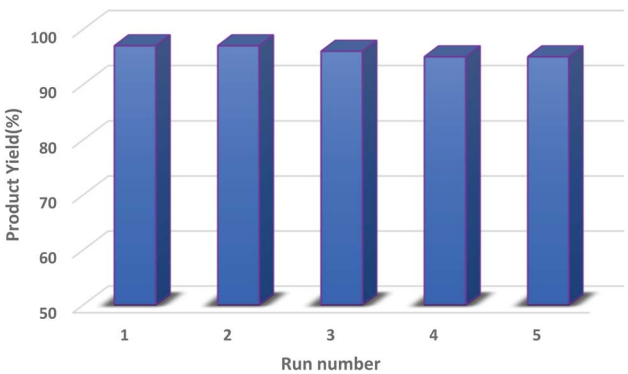

Fig. 10 Reusability of hercynite@SSA MNPs.

Table 3 Comparison of the catalytic activity of hercynite@SSA for the synthesis of bis(pyrazolyl)methanes with other reported catalyst systems in the literature

Entry	Catalyst	Conditions	Time	Yield[a] (%)	Ref.
1	[PEG–TEA]LP	Solvent-free, 60 °C	15	92	73
2	Aspirin	EtOH/H_2O, 60 °C	30	92	74
3	Nano-[Mn–4CSMP]Cl_2	Solvent-free, 100 °C	60	73	75
4	DCDBTSD	Solvent-free, 80 °C	40	80	76
5	SASPSPE	EtOH, reflux	132	85	77
6	Fe_3O_4@SiO_2@Si–$(CH_2)_3$@melamine	Solvent-free, 110 °C	9	88	78
7	[Et_3NH][HSO_4]	Solvent-free, 90 °C	30	87	79
8	DCDBTSD	Solvent-free, 80 °C	40	80	76
9	TMDP	EtOH, reflux	50	86	80
10	Hercynite@SSA	EtOH, reflux	120	97	This work

[a] Isolated yield.

catalytic systems are crucial subjects. The evaluation of this capability was carried out by performing a probe reaction and, after the completion of the reaction, the catalyst was recovered by magnetic decantation, washed properly with hot EtOH and acetone, and, finally, dried at 80 °C for 4 h. The dried catalyst was again used for the next cyclic runs of the mentioned transformations without adding any extra catalyst. The catalytic activity results of the reused catalyst are represented in Fig. 10. The depicted graphs in Fig. 8 show that, after 5 consecutive recycling, hercynite@SSA has the acceptable activity to promote the organic functional group transformation reactions.

3.2.4.2. Leaching and hot filtration tests. To illustrate the heterogeneous nature and structural stability of hercynite@SSA nanocatalyst, a hot filtration examination was carried out by performing probe reactions. After half time of the reaction (the reaction was progressed for 73%), the catalyst was magnetically separated from the reaction mixture under hot conditions. Afterward, the hot catalyst-free mixture was allowed to continue under similar transformation conditions for another half time of the reaction. In this sense, monitoring of the reaction indicates that the reaction did not show any significant change in yield. In addition, this examination confirms the heterogeneity of hercynite@SSA and the high stability of the chemosorbed acidic functionalities under the surface of the catalyst with negligible leaching.

3.2.5. Efficiency of hercynite/SSA (comparison). The comparative study of different catalytic protocols for the synthesis of 4,4'-(4-chlorophenylmethylene)-bis-(3-methyl-1-phenyl-1*H*-pyrazol-5-ol) as probe reaction is illustrated in Table 3. A case study shows that in terms of yield of the products, reaction time, and conditions, the hercynite@SSA represents a more environmentally friendly and comparable efficiency than the previously reported catalytic systems in the literature.

4. Conclusion

In summary, we have discovered a sustainable and convenient protocol for the synthesis of a novel inorganic sulfurous solid acid catalyst using a solid-state synthesis of silica sulfuric acid under the surface of magnetically recoverable hercynite. The FT-IR, XRD, TGA, DSC, EDX, X-ray-mapping, SEM, TEM, VSM and BET analyses confirm the core–shell structure of the as-prepared nanocomposite with the nanomagnetic hercynite as the core and amorphous phase of silica shell including SO_3H functionalities on its surface. Regarding the catalytic activity of this nanomagnetic solid acid catalyst, a green and economical procedure was developed for the synthesis of bis(pyrazolyl) methanes using two different synthetic methods. To promote the usefulness of the reaction, different arylated aldehydes with a high variety of structural differences were examined, and, accordingly, the pseudo-three-component method was faster and took lesser time than the pseudo-five-component synthetic methodology. The attractive features of the present protocol are the green approach, good yield, recovery of catalyst, and easy work-up procedure whereas the catalyst offers simple preparation, high catalytic activity, the quality of being easily used and inexpensive, recyclability, and good stability. The catalyst proved to be sustainable and recyclable for rapid synthesis of various heterocycles under green conditions.

Data availability

The data that support the findings of this study are available in the ESI† of this article.

Conflicts of interest

There are no conflicts to declare.

Acknowledgements

This work was supported by the research facilities of Ilam University, Ilam, Iran, and Bu-Ali Sina University, Hamedan, Iran.

References

1 M. Rahaman, M. S. Ali, K. Jahan, D. Hinz, J. Bin Belayet, R. Majinski and M. M. Hossain, *J. Org. Chem.*, 2021, **86**, 6138–6147.
2 X. Zhang, Z. Yang, Y. Jiang and S. Liao, *J. Am. Chem. Soc.*, 2022, **144**, 679–684.

3 T. Akiyama and K. Mori, *Chem. Rev.*, 2015, **115**, 9277–9306.
4 S. S. Patel, D. B. Patel and H. D. Patel, *ChemistrySelect*, 2021, **6**, 1337–1356.
5 L. J. Konwar, P. Mäki-Arvela and J.-P. Mikkola, *Chem. Rev.*, 2019, **119**, 11576–11630.
6 S. C. Datta, J. N. E. Day and C. K. Ingold, *J. Chem. Soc.*, 1939, 838.
7 B. Long, X.-F. Tan, C.-R. Chang, W.-X. Zhao, Z.-W. Long, D.-S. Ren and W.-J. Zhang, *J. Phys. Chem. A*, 2013, **117**, 5106–5116.
8 R. Kluger, F. Kerst, D. G. Lee, E. A. Dennis and F. H. Westheimer, *J. Am. Chem. Soc.*, 1967, **89**, 3718–3719.
9 S. Swann, R. D. Snow and D. B. Keyes, *Ind. Eng. Chem.*, 1930, **22**, 1048–1051.
10 K. Nakajima and M. Hara, *ACS Catal.*, 2012, **2**, 1296–1304.
11 P. Salehi, M. Dabiri, M. A. Zolfigol and M. A. Bodaghi Fard, *Tetrahedron Lett.*, 2003, **44**, 2889–2891.
12 M. A. Zolfigol, *Tetrahedron*, 2001, **57**, 9509–9511.
13 K. Niknam, H. Hashemi, M. Karimzadeh and D. Saberi, *J. Iran. Chem. Soc.*, 2020, **17**, 3095–3178.
14 A. Ghorbani-Choghamarani, H. Aghavandi and M. Mohammadi, *J. Porous Mater.*, 2021, **28**, 1167–1186.
15 A. Pramanik and S. Bhar, *Catal. Commun.*, 2012, **20**, 17–24.
16 M. Mohammadi, M. Khodamorady, B. Tahmasbi, K. Bahrami and A. Ghorbani-Choghamarani, *J. Ind. Eng. Chem.*, 2021, **97**, 1–78.
17 M. Kazemi and M. Mohammadi, *Appl. Organomet. Chem.*, 2020, **34**, e5400.
18 Q. Zhang, X. Yang and J. Guan, *ACS Appl. Nano Mater.*, 2019, **2**, 4681–4697.
19 Z. Ma, J. Mohapatra, K. Wei, J. P. Liu and S. Sun, *Chem. Rev.*, 2021, DOI: **10.1021/acs.chemrev.1c00860**.
20 S. Esmaili, A. Khazaei, A. Ghorbani-Choghamarani and M. Mohammadi, *RSC Adv.*, 2022, **12**, 14397–14410.
21 F. Ghobakhloo, D. Azarifar, M. Mohammadi and M. Ghaemi, *Appl. Organomet. Chem.*, 2022, e6823.
22 P. M. Martins, A. C. Lima, S. Ribeiro, S. Lanceros-Mendez and P. Martins, *ACS Appl. Bio Mater.*, 2021, **4**, 5839–5870.
23 N. Rezvani Jalal, P. Mehrbod, S. Shojaei, H. I. Labouta, P. Mokarram, A. Afkhami, T. Madrakian, M. J. Los, D. Schaafsma, M. Giersig, M. Ahmadi and S. Ghavami, *ACS Appl. Nano Mater.*, 2021, **4**, 4307–4328.
24 S. Wang, J. Xu, W. Li, S. Sun, S. Gao and Y. Hou, *Chem. Rev.*, 2022, **122**, 5411–5475.
25 A. Ghorbani-Choghamarani, M. Mohammadi, L. Shiri and Z. Taherinia, *Res. Chem. Intermed.*, 2019, **45**, 5705–5723.
26 R. Mistri, S. Maiti, J. Llorca, M. Dominguez, T. K. Mandal, P. Mohanty, B. C. Ray and A. Gayen, *Appl. Catal., A*, 2014, **485**, 40–50.
27 N. J. Morales, S. Goyanes, C. Chiliotte, V. Bekeris, R. J. Candal and G. H. Rubiolo, *Carbon*, 2013, **61**, 515–524.
28 J. Li, J. Zhang, S. Wang, G. Xu, H. Wang and D. G. Vlachos, *ACS Catal.*, 2019, **9**, 1564–1577.
29 X. Xu, J. Enchen, W. Mingfeng, L. Bosong and Z. Ling, *Renewable Energy*, 2012, **41**, 23–28.
30 R. M. Trottier, Z. J. L. Bare, S. L. Millican and C. B. Musgrave, *ACS Appl. Mater. Interfaces*, 2020, **12**, 23831–23843.
31 S. L. Millican, J. M. Clary, C. B. Musgrave and S. Lany, *Chem. Mater.*, 2022, **34**, 519–528.
32 M. Mohammadi and A. Ghorbani-Choghamarani, *New J. Chem.*, 2020, **44**, 2919–2929.
33 M. Mohammadi and A. Ghorbani-Choghamarani, *RSC Adv.*, 2022, **12**, 2770–2787.
34 M. Mohammadi and A. Ghorbani-Choghamarani, *Res. Chem. Intermed.*, 2022, **48**, 2641–2663.
35 S. Kar, H. Sanderson, K. Roy, E. Benfenati and J. Leszczynski, *Chem. Rev.*, 2022, **122**, 3637–3710.
36 H. Yazdani, S. E. Hooshmand and R. S. Varma, *ACS Sustainable Chem. Eng.*, 2021, **9**, 16556–16569.
37 L. Zeng, B. Huang, Y. Shen and S. Cui, *Org. Lett.*, 2018, **20**, 3460–3464.
38 M. Pinaud, E. Huet, M. Presset and E. Le Gall, *J. Org. Chem.*, 2022, **87**(7), 4971–4980.
39 G. Rahimzadeh, M. Tajbakhsh, M. Daraie and M. Mohammadi, *Appl. Organomet. Chem.*, 2022, e6829, DOI: **10.1002/aoc.6829**, article in press.
40 A. Ghorbani-Choghamarani, M. Mohammadi, T. Tamoradi and M. Ghadermazi, *Polyhedron*, 2019, **158**, 25–35.
41 F. Ghobakhloo, D. Azarifar, M. Mohammadi, H. Keypour and H. Zeynali, *Inorg. Chem.*, 2022, **61**, 4825–4841.
42 G. An and G. Li, in *Domino Reactions*, Wiley-VCH Verlag GmbH & Co. KGaA, Weinheim, Germany, 2013, pp. 141–182.
43 T. Tamoradi, M. Mohammadi, A. R. Kiasat, J. Davarpanah and B. Karmakar, *Polycyclic Aromat. Compd.*, 2021, **150**, 1–15.
44 P. Seguí, J. J. Aguilera-Correa, E. Domínguez-Jurado, C. M. Sánchez-López, R. Pérez-Tanoira, A. V Ocaña, J. A. Castro-Osma, J. Esteban, A. Marcilla, C. Alonso-Moreno, F. C. Pérez-Martínez and M. Molina-Alarcón, *Sci. Rep.*, 2021, **11**, 16306.
45 A. Mustafa, S. Siddiqui, M. Umar Khan, A. A. Qasem Ali and Z. N. Siddiqui, *ChemistrySelect*, 2021, **6**, 8611–8629.
46 M. Sadeghpour and A. Olyaei, *Recent advances in the synthesis of bis(pyrazolyl)methanes and their applications*, Springer Netherlands, 2021, vol. 47.
47 H. Filian, A. Kohzadian, M. Mohammadi, A. Ghorbani-Choghamarani and A. Karami, *Appl. Organomet. Chem.*, 2020, **34**, e5579.
48 T. Tamoradi, S. M. Mousavi and M. Mohammadi, *New J. Chem.*, 2020, **44**, 8289–8302.
49 U. Kurtan and A. Baykal, *Mater. Res. Bull.*, 2014, **60**, 79–87.
50 H. Liu, H. Li, Z. Ding, A. Fu, H. Wang, P. Guo, J. Yu, C. Wang and X. S. Zhao, *J. Cluster Sci.*, 2012, **23**, 273–285.
51 V. Umamaheswari, *J. Catal.*, 2002, **210**, 367–374.
52 F. Hajizadeh, A. Amiri, B. Maleki and F. Mohammadi Zonoz, *Microchem. J.*, 2022, **175**, 107176.
53 J. P. Misiewicz, K. B. Moore, P. R. Franke, W. J. Morgan, J. M. Turney, G. E. Douberly and H. F. Schaefer, *J. Chem. Phys.*, 2020, **152**, 024302.
54 A. Tambe, A. Gadhave, A. Pathare and G. Shirole, *Sustainable Chem. Pharm.*, 2021, **22**, 100485.
55 E. J. Verwey, P. W. Haayman and F. C. Romeijn, *J. Chem. Phys.*, 1947, **15**, 181–187.

56 N. Kurnaz Yetim, F. Kurşun Baysak, M. M. Koç and D. Nartop, *J. Mater. Sci.: Mater. Electron.*, 2020, **31**, 18278–18288.
57 T. Kjällman and I. Olovsson, *Acta Crystallogr., Sect. B: Struct. Crystallogr. Cryst. Chem.*, 1972, **28**, 1692–1697.
58 J. Wang, S. Zheng, Y. Shao, J. Liu, Z. Xu and D. Zhu, *J. Colloid Interface Sci.*, 2010, **349**, 293–299.
59 E. Karaoğlu, H. Deligöz, H. Sözeri, A. Baykal and M. S. Toprak, *Nano-Micro Lett.*, 2011, **3**, 25–33.
60 I.-G. Athanasoulia and P. A. Tarantili, *Pure Appl. Chem.*, 2017, **89**, 141–152.
61 A. R. Kiasat and J. Davarpanah, *Res. Chem. Intermed.*, 2015, **41**, 2991–3001.
62 H. Naeimi and S. Mohamadabadi, *Dalton Trans.*, 2014, **43**, 12967–12973.
63 H. R. Shaterian, M. Ghashang and M. Feyzi, *Appl. Catal., A*, 2008, **345**, 128–133.
64 K. Tanabe, M. Misono, Y. Ono, and H. Hattori, in *New Solid Acids and Bases*, Elsevier, 1989, vol. 51, pp. 5–25.
65 K. Niknam and S. Mirzaee, *Synth. Commun.*, 2011, **41**, 2403–2413.
66 M. Keshavarz and M. Vafaei-Nezhad, *Catal. Lett.*, 2016, **146**, 353–363.
67 M. Makvandi, F. A. Dil, A. Malekzadeh, M. Baghernejad and K. Niknam, *Iran. J. Catal.*, 2013, **3**, 221–228.
68 M. Baghernejad and K. Niknam, *Int. J. Chem.*, 2012, **4**, 52–60.
69 M. A. Zolfigol, M. Navazeni, M. Yarie and R. Ayazi-Nasrabadi, *Appl. Organomet. Chem.*, 2017, **31**(6), e3633.
70 H. Filian, A. Ghorbani-Choghamarani and E. Tahanpesar, *J. Iran. Chem. Soc.*, 2019, **16**, 2673–2681.
71 M. A. Zolfigol, R. Ayazi-Nasrabadi and S. Baghery, *RSC Adv.*, 2015, **5**, 71942–71954.
72 K. Niknam, M. S. Habibabad, A. Deris and N. Aeinjamshid, *Monatsh. Chem.*, 2013, **144**, 987–992.
73 R. Kordnezhadian, M. Shekouhy, S. Karimian, Z. Tavaf, S. Malek-Hosseini, M. B. Shahsavani, Z. Amirghofran, R. Yousefi and A. Khalafi-Nezhad, *New J. Chem.*, 2020, **44**, 16995–17012.
74 M. Fatahpour, F. Noori Sadeh, N. Hazeri, M. T. Maghsoodlou and M. Lashkari, *J. Iran. Chem. Soc.*, 2017, **14**, 1945–1956.
75 A. R. Moosavi-Zare, H. Goudarziafshar and S. Dastbaz, *J. Chin. Chem. Soc.*, 2017, **64**, 727–731.
76 A. Khazaei, F. Abbasi and A. R. Moosavi-Zare, *New J. Chem.*, 2014, **38**, 5287–5292.
77 S. Tayebi, M. Baghernejad, D. Saberi and K. Niknam, *Cuihua Xuebao*, 2011, **32**, 1477–1483.
78 M. Soleimani, A. Khazaei, N. Sarmasti and T. Akbarpour, *J. Iran. Chem. Soc.*, 2022, **19**(5), 1849–1863.
79 Z. Zhou and Y. Zhang, *J. Chil. Chem. Soc.*, 2015, **60**, 2992–2996.
80 N. G. Khaligh and T. Mihankhah, *J. Heterocycl. Chem.*, 2020, **57**, 4036–4043.